

New x-ray tube performance in computed tomography by introducing the rotating envelope tube technology

Peter Schardt,^{a)} Josef Deuringer, Jörg Freudenberger, Erich Hell,^{b)} Wolfgang Knüpfer, Detlef Mattern, and Markus Schild

Siemens Medical Solutions, Vacuum Technology, Erlangen, Germany

(Received 30 January 2004; revised 16 June 2004; accepted for publication 28 June 2004; published 27 August 2004)

The future demands of computed tomography imaging regarding the x-ray source can be summarized with higher scan power, shorter rotation times, shorter cool down times and smaller focal spots. We report on a new tube technology satisfying all these demands by making use of a novel cooling principle on one hand and of a novel beam control system on the other hand. Nowadays tubes use a rotating anode disk mainly cooled via radiation. The Straton[®] x-ray tube is the first tube available for clinical routine utilizing convective cooling exclusively. It is demonstrated that this cooling principle makes large heat storage capacities of the anode disk obsolete. The unprecedented cooling rate of 4.8 MHU/min eliminates the need for waiting times due to anode cooling in clinical workflow. Moreover, an electronic beam deflection system for focal spot position and size control opens the door to advanced applications. The physical backgrounds are discussed and the technical realization is presented. From this discussion the superior suitability of this tube to withstand g-forces well above 20 g created by fast rotating gantries will become evident. Experience from a large clinical trial is reported and possible ways for future developments are discussed. © 2004 American Association of Physicists in Medicine. [DOI: 10.1118/1.1783552]

Key words: x-ray tubes, anode cooling, electron beam, cardiac CT

I. INTRODUCTION

Medical x-ray diagnostics makes use of two types of x-ray tubes. For low power applications stationary anode tubes are the best compromise between technical design effort and performance. But for most midrange and high performance applications in terms of focal spot power there is a need to utilize rotating anode tubes. These tubes provide a focal spot power of 60–100 kW for computed tomography (CT) as well as angiography. Especially in CT, large amounts of dissipated energy are produced by patient scans in the order of some ten seconds. In contrast to the stationary anodes the heat has to be stored in the anode disk and has to be transferred by radiation at high temperatures to the cooling medium. The main components of such a tube can be seen from Fig. 1 (taken from Ref. 1). As a consequence of this bottleneck for the heat flow, the anode has to store nearly the complete amount of energy up to several MJ (or expressed in the more common unit Mega Heat Unit, MHU, where 1 MJ equals 1.34 MHU). The reason is illustrated in Fig. 2. The temperature in the focal spot is limited by the material used and for medical tubes somewhere below the melting point of tungsten. This temperature for rotating anodes is a composition of the anode disk temperature and the short temperature rise of the material passing the target spot of the electron beam. The temperature rise is a function of material properties, focal spot size, focal spot power and the velocity of the material (for rotating anodes a function of radius and rotating frequency). In contrast the disk temperature is determined by the heat capacity and the applied cooling mechanism. Many improvements to cool the disk deal with enhanced emissivity ε or increased areas A_R of radiation emitting and absorbing

surfaces (optimized for x-ray tubes, e.g., in Ref. 2). The goal is to maximize the heat flow P_R given by the Stefan–Boltzmann³ radiation law,

$$P_R = \varepsilon \cdot A_R \cdot (T_A^4 - T_H^4), \quad (1)$$

with T_A being the temperature of the anode and T_H the temperature of the housing. Few attempts have also been made to introduce convective cooling by using liquid metal to bear the anode disk and achieve a modest improvement of the cooling.⁴ Cooling rates of up to 1.4 MHU/min have been reported.⁵ However, for a further increase of cooling rates one possibility is to get the anode disk itself in contact to the cooling medium. One solution for that is a design where the anode disk is part of the tube envelope. This implies rotation of the entire tube with respect to the anode axis, which we refer to as the class of rotating envelope tubes (RET) in contrast to the rotating anode tubes, where the tube envelope is stationary. The Straton tube (Siemens Medical Solutions, Erlangen, Germany) is the first tube based on this technology introduced into the high performance class of computed tomography with outstanding power reserves.

Physical details of convective cooling and beam control are discussed in Sec. II: the impact on the technical realization is presented in Sec. III. We report the results from a large clinical field trial in Sec. IV before an outlook to future developments is given in the concluding section (Sec. V).

II. PRINCIPLE AND PHYSICAL ASPECTS

A very early appearance of the idea to rotate the tube envelope and deflect an electron beam by stationary means is

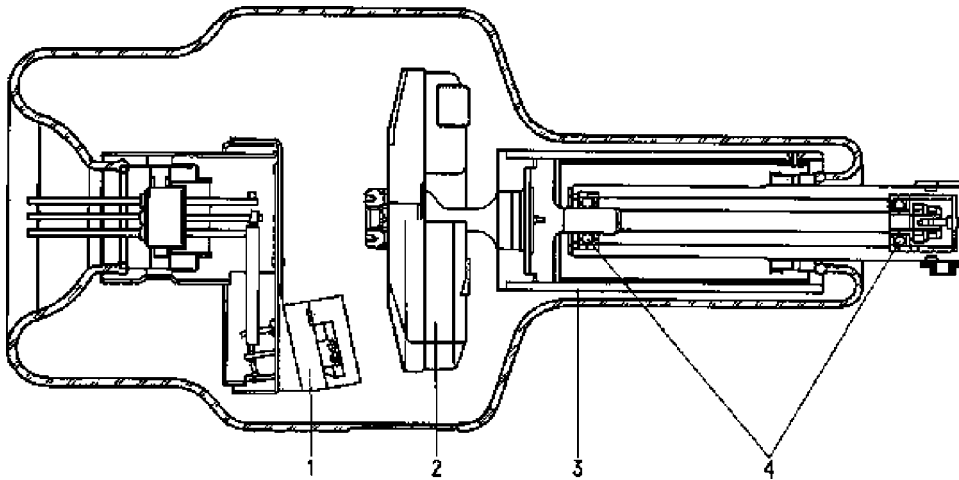


FIG. 1. Main parts of a medical diagnostic x-ray tube (1: cathode, 2: anode, 3: rotor, 4: ball bearings, as taken from Ref. 1). The large anode disk has to store the heat generated during the exposure and radiates at very high temperatures to cool down in the intermediate times.

first documented in a patent of 1917.⁶ This design is in fact very close to the realized Straton tube. Within this principle, the electron beam in the tube is shaped and controlled by a magnetic field similar to a miniature electron beam CT. In Fig. 3 one can recognize the vacuum housing rotating in bearings outside the vacuum and driven by an external motor. The tube housing itself consists of a cathode shaft, a ceramic high voltage insulator, a tube envelope, an annular x-ray window and the anode disk mounted on a second shaft. For running the tube, a drive motor is attached to the anode shaft and a magnetic deflection system is positioned in the plane of the tube waist to deflect the electron beam onto the focal spot position. In the following we discuss the physical aspects of the two major differences between rotating envelope tubes and rotating anode tubes, namely the thermodynamics in Sec. II A and the electron beam dynamics in Sec. II B.

A. Thermodynamics

In this concept the cooling surface of the anode is in direct contact with the cooling fluid. The heat transfer for the so called convective cooling P_C is given by

$$P_C = \alpha \cdot A_C \cdot \Delta T, \quad (2)$$

where P_C is the transferred power, α the heat transfer coefficient, A_C the cooling surface and ΔT the temperature difference between cooling surface and cooling fluid. The largest values of α are achieved for turbulent flow, because the turbulence causes additional material transport in the direction perpendicular to the cooling surface.⁷ With the help of FEM-calculations (numerical computer simulations using finite element methods) one can derive values of $36.000 \text{ W/m}^2\text{K}$ for an anode disk of 60 mm radius and a rotating speed of 150 Hz , as illustrated in Fig. 4. To obtain a rough estimation for the heat flow, one can insert numbers in Eq. (2) for the cooling surface area (85 cm^2), the temperature difference (250 K) and a mean α of $30.000 \text{ W/m}^2\text{K}$ to end up with a heat transfer rate of more than 60 kW directly transferred to the cooling fluid. This value corresponds to an unprecedented cooling rate of 4.8 MHU/min compared to state of the art performances of $0.8\text{--}1.4 \text{ MHU/min}$. Looking at Fig. 5 one can recognize that in 20 s the anode is completely cooled down to the oil temperature. The cool down time for a radiation cooled anode is also visible. With this example it

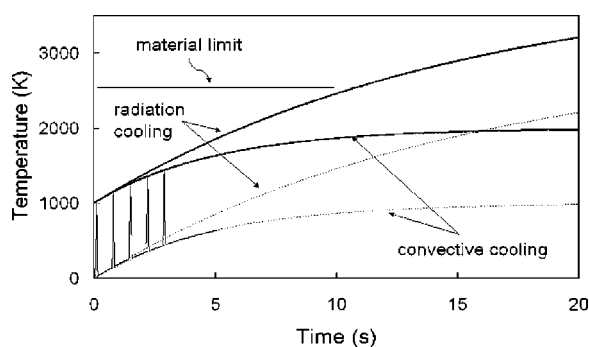


FIG. 2. Temperatures of anode disk (dotted) and focal spot (solid) for a specific applied electrical power at the focal spot. The comparison exhibits the difference in temporal behavior for a rotating anode tube (radiation cooling) and a corresponding rotating envelope tube (convective cooling). Numerical values are for illustration only.

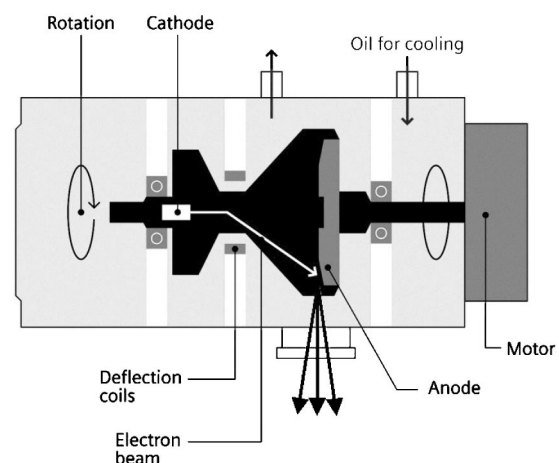


FIG. 3. Principle of operation and main parts of a RET housing assembly.

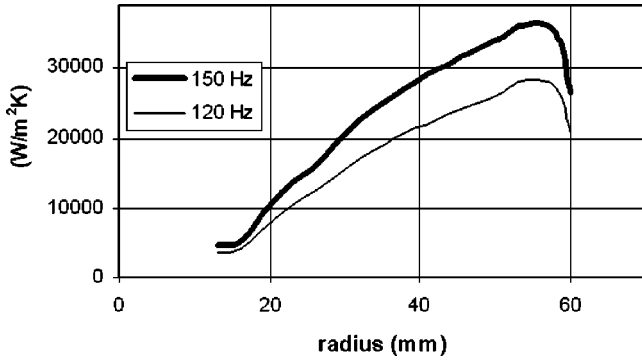


FIG. 4. Local heat transfer coefficient α as a function of distance from the axis calculated for the Straton geometry with a tube radius of 60 mm. The radius of the focal track is 48 mm. Data are given for two rotating frequencies and are obtained by a fluid dynamical FEM simulation.

becomes clear that there is no need for a large heat storage capacity at the anode any longer. However, a small amount is still needed for the anode to act as a heat spreader from the area of the focal spot to the large area of the cooling surface.

Using this setup, the rotation of the anode serves a dual-purpose: inside of the tube the rotation maintains a tolerable focal spot temperature rise, outside of the tube the rotation causes turbulent oil flow to maintain large heat transfer coefficients.

Nevertheless, the requirements of turbulence and rotation speed result in a substantial amount of dissipated frictional power which has to be provided by the external motor. In the following we describe a way to reduce the drive power by geometrical implications. The functional dependencies of the frictional power on geometric and physical properties of the rotating part can be explained by^{8,9}

$$P_{drive} \propto \rho \nu^{0.2} \cdot h R_{tube}^{3.9} d^{-0.3} \cdot f^{2.8}, \quad (3)$$

where P_{drive} is the driving power, ρ the density and ν the cinematic viscosity of the fluid and f the rotational frequency. Equation (3) has been derived for a solid cylinder of radius R_{tube} and height h rotating in a stationary cylinder. The rotating cylinder and the fixed surrounding housing (stationary cylinder) define an intermediate volume between the cylinders of thickness d , where the friction in the fluid is gener-

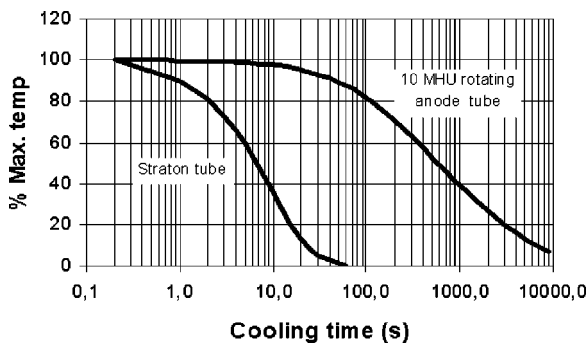


FIG. 5. Cooling curve comparison with data from time resolved FEM calculations. Upper curve for rotating anode tube; lower curve for the Straton anode.

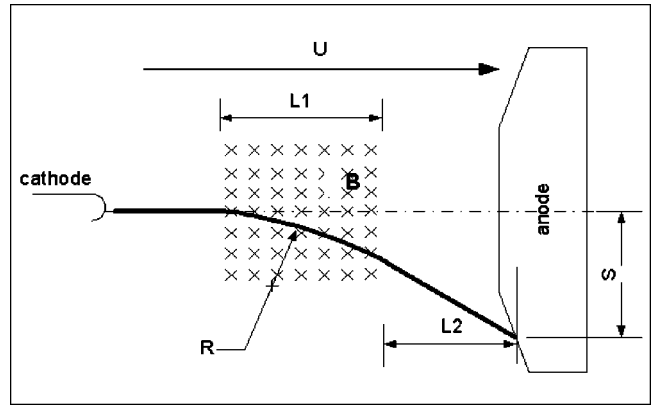


FIG. 6. Simplified model to calculate the required magnetic field strength B for a given geometry and accelerating voltage U . The magnetic field bends the beam with curvature radius R over the length $L1$. After the field free section of length $L2$ the electrons hit the anode at the focal spot position.

ated. From Eq. (3) it becomes clear that there is a strong dependency on the tube radius and the rotational frequency. The viscosity of the fluid and the width of the slit have only a minor impact. A major task for keeping drive power low is therefore an optimization of the radial dimensions of the geometry. As a result of this we found a very compact double cone shaped design described in detail in Sec. III. In particular we found other solutions to realize a rotating envelope tube (for example, a tube with a beared and magnetically fixed cathode¹⁰) to exhibit much larger drive power for a given anode diameter and rotating frequency, because a large radius R_{tube} has to be maintained over a long height h .

B. Electron beam dynamics

The second physical aspect covers the requirements for the electron beam deflection and focusing. To achieve an x-ray focal spot fixed in space while the whole tube is rotating, a stationary beam deflection system is necessary. In the easiest way this is achieved by a dipole magnet system deflecting the electron beam generated on the tube axis such that the beam hits the anode disk exactly at the focal spot position of the tube housing assembly. In the tube voltage range used for medical imaging of about 40 kV to 150 kV, the electrons gain a speed up to about 50% of the speed of light. Therefore, the Lorentz force has to be calculated using the relativistic electron mass and is nonlinear in this range. The basic formula for the deflection of the electron beam will be found by the basic equations for the Lorentz force and the centrifugal force. The result is the curvature radius R of the electrons,

$$R = \frac{mv}{e_0 B}, \quad (4)$$

with m being the relativistic mass of an electron accelerated by the voltage U . Using a simple model (see Fig. 6), the distance S of the focal spot from the rotation center (=focal track radius) depends only on the geometric data and radius R ,

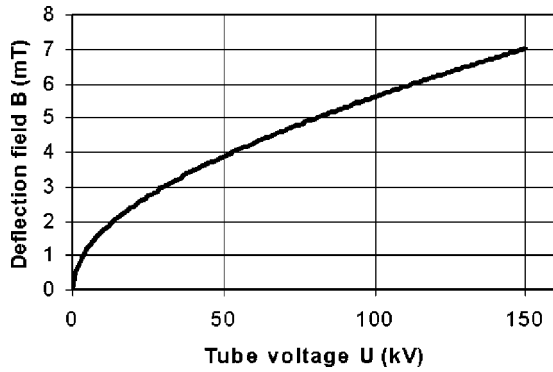


FIG. 7. Field strength for magnetic beam deflection system as function of tube voltage U.

$$S = \left(1 - \sin \left(a \cos \left(\frac{L_1}{R} \right) \right) \right) \cdot R + \frac{L_2}{\tan \left(a \cos \frac{L_1}{R} \right)}. \quad (5)$$

Using Eqs. (4) and (5) we obtain the required magnetic field strength B for a given deflection S, which is plotted as a function of the tube voltage U in Fig. 7.

Despite the nonlinear function for the deflection field an additional aspect complicates the situation. The electron beam length (way of electrons from emitter to the focal spot) is about 115 mm and therefore considerably longer than in conventional x-ray tubes (see for example Fig. 1, where the beam length is about 30 mm). This is due to the fact that the beam is created on the rotational axis of the tube, accelerated in the direction of the axis and then deflected to the position given by the focal track radius. As a consequence thereof, space charge effects play an important role, because the electrons are not fully relativistic. The electric and magnetic fields within a long beam with cylindrical symmetry and radius r are¹¹

$$E_r = \frac{1}{\epsilon_0 r} \int_0^r r' \rho(r') dr', \quad (6a)$$

$$B_\varphi = \frac{\mu_0}{r} \int_0^r r' j(r') dr'. \quad (6b)$$

Upon an individual charge, these fields inflict repulsive and attractive forces, respectively, according to the basic equation of motion,

$$\frac{d}{dt} (m \cdot \vec{v}) = q \vec{E} + q \vec{v} \times \vec{B}. \quad (7)$$

Inserting (6a), (6b) into (7) one ends up with the resulting radial force,

$$F_{\text{tot}} = \frac{q}{r v \epsilon_0} [1 - \beta^2] \cdot \int_0^r r' j(r') dr', \quad (8)$$

which is defocusing for all but highly relativistic particles ($\beta = v/c$, the fractional speed of light). From (7) and (8), a trajectory equation can be derived under the assumption of a homogeneous radial current density. With constant current

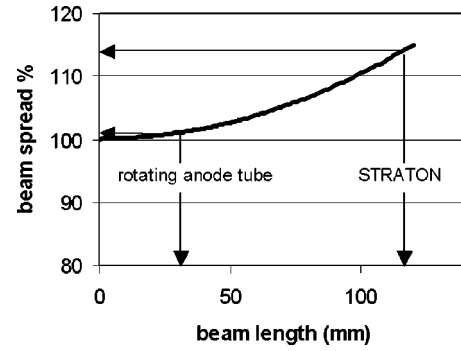


FIG. 8. Beam spread for an electron beam calculated with an initial radius of 2.5 mm at the emitter as a function of beam length (100% is the beam diameter at the emitter) in comparison for rotating anode tubes (typical value) and a RET (120 kV tube voltage and 500 mA beam current).

and energy, one can furthermore generate the envelope equation, which gives the beam radius R_{beam} as a function of z in the implicit form

$$\frac{d^2}{dz^2} R_{\text{beam}}(z) = \frac{qI}{2\pi\epsilon_0 m_0 (\gamma\beta c)^3} \cdot \frac{1}{R_{\text{beam}}(z)}. \quad (9)$$

This differential equation (9) can be solved numerically and R_{beam} is plotted in Fig. 8. It can be seen that for the given beam parameters a beam with a large beam length like in a RET is much more spread than in a conventional rotating anode tube. However, this calculation example is only for illustration, because none of the given ideal assumptions is accomplished in the real tube. In the Straton tube the acceleration, deflection and focusing of the beam are not separated in space. Properties of the real beam (e.g., beam size at focal spot position) have therefore to be calculated with FEM calculations.

Tube current and voltage are determined by the application and therefore variable. Both are selected in order to optimize CT image quality with respect to the given attenuation properties of the human body. To maintain a certain range of operation with stable focal properties, one needs additional focusing in order to compensate F_{tot} . To supply this additional force, a quadrupole component of the magnetic field may be used in addition to the dipole component of the deflection field. The calculation of the electron trajectories under the influence of these superimposed magnetic field components, while the electrons are accelerated simultaneously, is easily done by FEM calculations even under consideration of the space charge effects. An example for such a calculation is given in Fig. 9. Ignoring the vacuum envelope of the tube, the tracks of the electrons are visible starting at the emitter and traveling through the magnetic deflection and focusing field before reaching the anode at the focal spot.

III. TECHNICAL REALIZATION

Although the idea of turning the tube housing is very old and the underlying physics is easily understandable, this technology did not find its way to routine medical imaging before 2003. This is mainly because of some obstacles in

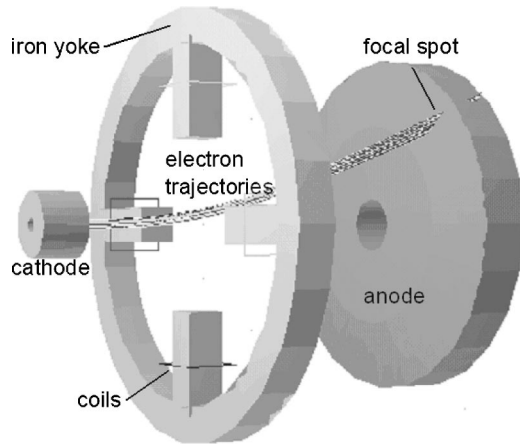


FIG. 9. FEM calculation of electron trajectories from the cathode through the complex magnetic deflection and focusing field to the focal spot at the anode.

technical realization, which had to be overcome. From image quality requirements on focal spot stability a need for an intelligent beam control can be derived. Position and stability in shape are crucial especially in computed tomography. Therefore a microcontroller is essential, in particular considering the mostly nonlinear dependencies as discussed before. However, also mechanical aspects have to be taken into account. High performance tubes have to run at very high rotation speeds and one can imagine, that the traditional glass tube technology is not adequate in terms of required precision and stability. Since the early nineties, the metal ceramic technology is routinely used for medical tubes with highest power demands and is a key factor for manufacturing reliable rotating envelope tubes.

Out of these reasons, we describe the realization and discuss some properties of the key components of the Straton tube, namely the tube envelope in Sec. III A and the filament for electron emission in Sec. III B. In Sec. III C we deal with the magnetic deflection system and in Sec. III D with the cooling system.

A. Tube envelope

In Fig. 10 the Straton tube is shown with an anode disk of 120 mm diameter capable to rotate at 150 Hz. The tube envelope made of nonmagnetic stainless steel is attached to the anode disk made of a tungsten zirconium molybdenum body equipped with a tungsten rhenium focal spot track including an annular x-ray window of 0.2 mm thickness¹² made out of stainless steel. In contrast to all other x-ray tubes, the window is rotating through the x-ray beam and has to be extremely uniform in terms of x-ray attenuation. On the cathode side, a ceramic disk insulator ensures a reliable high voltage insulation of about 170 kV in the vacuum (inside) as well as in the cooling oil (outside). The geometries of all the components were chosen very carefully in order to keep the drive power acceptable. The power required to maintain the rotation and turbulent flow of the insulating oil at the maximum rotational speed of 150 Hz does not exceed 6–7 kW. To keep frictional power losses low, the vacuum housing is ac-

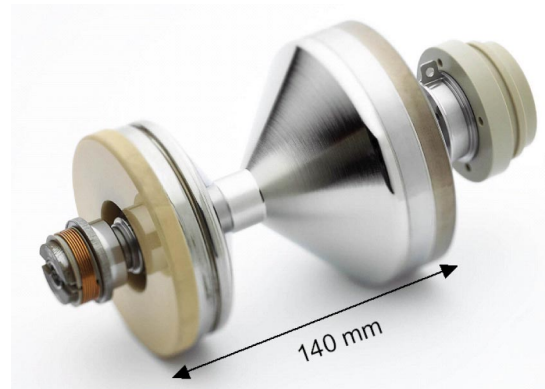


FIG. 10. The Straton tube with a cathode and ceramic insulator at the left and an anode at the right. Ball bearings are mounted as well as the inductive filament transformer. The largest diameter of the tube is 120 mm.

celerated (in about half a second) to this high speed only when the maximum electron beam power is impinging the anode. All other applications run at lower rotating frequencies with an intelligent power management. Therefore, the average driving power can be kept below a level of 500–600 W only.

B. Electron emission

Much attention has to be spent on the filament. Ideally, a circular uniform emission is needed to avoid unwanted rotational focal spot size modulations, which may reduce image quality in computed tomography. Our tube uses a circular emitter made of 100 μm thick tungsten sheet material, which is cut by the laser in a way to form meander like paths for the filament heating current.¹³ In Fig. 11 one can recognize the structure of the flat emitter inside the focusing device.

This flat emitter technology has important advantages concerning high speed dose variations during fast CT-scans. The limiting parameter for fast emission changes is the cooling time of the emitter. Assuming radiation cooling only, at high temperatures ($>2000^\circ\text{C}$) the rate of change for the emitter temperature T is given by



FIG. 11. Details of the Straton cathode. Inside the focusing head, the emitter made of tungsten sheet is visible. The emitter has a diameter of 5 mm.

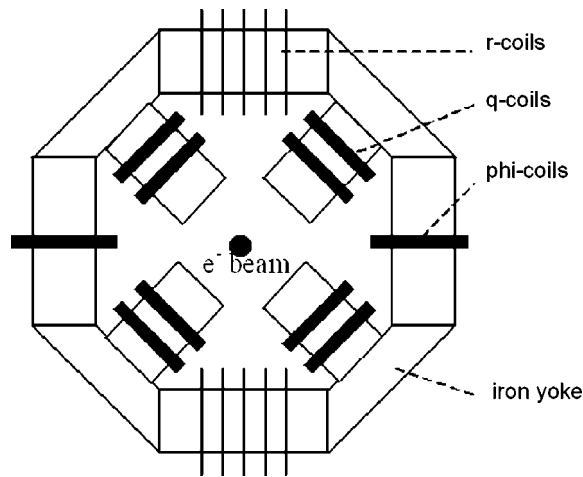


FIG. 12. Scheme of the magnet system with different coils.

$$\frac{dT}{dt} = \frac{1}{c_s m_E} \cdot \dot{Q}, \quad (10)$$

with c_s and m_E denoting the specific heat capacity, mass and \dot{Q} the rate of change of the thermal energy. Taking into account, that the temporal change of Q is caused by radiation and equals therefore the radiated Power P_R given by Eq. (1), one ends up with

$$\frac{dT_E}{dt} = \frac{\varepsilon}{c_s} \cdot \frac{A_E}{m_E} (T_E^4 - T_S^4), \quad (11)$$

A_E being the area of the radiating surfaces, T_E and T_S the temperatures of the emitter and the surrounding surfaces, respectively. The rate of temperature decline is dependent on the geometry factor A_E/m_E for a given material (ε and c_s) only. Inserting values for a typical helical tungsten wire emitter ($A_E=93 \text{ mm}^2, m_E=250 \text{ mg}$) and comparing them with the new developed flat emitter ($A_E=40 \text{ mm}^2, m_E=37 \text{ mg}$), a factor of three is gained in variation speed. This is in good agreement with measurements. For dose management in clinical applications, this is a crucial benefit in achieving an accurate dose profile as a function of gantry rotation, in particular for highest rotating speeds in cardiology.

The tube rotating in lubricated ball bearings has an inductive heat transformer, which transmits the filament heating power from a stationary primary coil to the rotating secondary coil (visible in Fig. 10) to avoid any degradation of the insulation oil.

C. Magnetic deflection system

The deflection system has to perform three tasks: first the deflection of the beam in the radial direction onto the focal spot and to perform a flying focal spot in the z -direction; second the focusing of the beam to determine the size of the electronic focal spot; and third a deflection to make use of a flying focal spot in the ϕ -direction. For this purpose a magnet design similar to a quadrupole is chosen of which Fig. 12 gives a schematic sketch. In contrast to a pure quadrupole magnet, the Straton magnet system has three different sets of

TABLE I. Three electronically adjusted sizes for the focal spots of Straton and their maximum load (for 20 s).

Focal spot	Spot size (w×l, IEC 60336 values)	Maximum load (20 s scantime)
F I	0.6×0.7	42 kW
F II	0.8×0.8	51 kW
F III	0.8×1.2	60 kW

coils¹⁴ corresponding to the three tasks mentioned above. The r -coils generate the main dipole component of the magnetic field to deflect the beam onto the focal spot, which is quasistatic in time disregarding the switching when the tube voltage is turned on or off. The focusing is performed by four q -coils generating a quadrupole component used for forming the electronic focal spot. The third setup (ϕ -coils) are used to produce a small but fast dipole component for the flying focal spot in the tangential direction. Because all the coil currents depend on the value of the high voltage used in the way as described in Sec. II, a microcontroller drives individual current power amplifiers for each coil setup. The microcontroller calculates the required coil current in real time as a function of the measured high voltage. For each focal spot size, a set of coil current tables is managed by the microcontroller. So, an electronically adjustable focal spot is realized having the advantages of low tolerances in spot size dimensions, fast switching and high flexibility.¹⁵ For example, our RET uses three different focal spot sizes with only one emitter, which can be used to adapt to the best image quality possible. Table I illustrates the variety of the spot sizes for Straton.

D. Cooling system

The cooling system used for transferring the heat from the oil to the gantry air is designed for the large centrifugal forces at gantry rotation times of 0.37 s per revolution and is capable of cooling oil temperatures of about 100 °C. To avoid any cavitation in the oil due to the fast rotating tube, which may result in a reduced high voltage stability, the cooling system works at a pressure of about 1 bar. Although there is an oil pump in the system, the main oil flow is caused by the rotating tube.¹⁶ We measured 25 L/min when the tube is rotating, resulting in a very effective cooling in contrast to 8 L/min with only the oil pump running. The oil to air heat exchanger is designed to cool down a continuous power of 7 kW, which is appropriate for high performance CT. However, this heat exchanger is the bottleneck for the maximum continuous power now. While the heat from the anode is directly transferred to the cooling oil, it has to be stored by the heat capacity of the oil contained by the tube housing assembly and the cooling system, until it is again cooled down by the gantry air. In this situation the average power is only determined by the cooling capacity of the heat exchanger. Therefore, in principle much larger average power would be possible with an appropriate design of the cooling system.



FIG. 13. Cardiac scanning at 0.37 s per revolution demonstrating the superior resolution applied to the beating heart (courtesy of Dr. A. Küttner, Univ. of Tübingen, Germany).

IV. PERFORMANCE RESULTS AND CLINICAL FIELD TRIAL

The Straton tube was intensively tested in a clinical field trial on the SOMATOM Sensation 16 scanner (Siemens Medical Solutions, Forchheim, Germany). About 25 installations running from Feb/03 to Oct/03 were monitored online via remote control to observe the clinical performance.

The installations with these tubes exhibited essentially no tube cooling times, confirming the difference in the tube cooling performance. One clinic is running the tube at 45.000 scanseconds per month with about 50–60 patients per day. An impressive number for the demonstration of a workflow no longer limited by waiting times due to tube cooling. The focal spot F II (medium size, see Table I) was used for more than 90% of all scans, resulting in a statement that 50 kW scanpower is appropriate for routine examination. An UHR-mode (ultra high resolution mode) utilizing the FI as well as the high power modes were only used in a few cases.

The Straton tube is the first tube routinely used at a gantry revolution time of 0.37 s. This mode was used for all cardiac

TABLE II. Centrifugal forces at tube axis as function of gantry rotation speed.

Gantry revolution time	Centrifugal acceleration on tube axis (650 mm) in units of g ($=9.81 \text{ m/s}^2$)
1 s	3
0.5 s	10
0.4 s	16
0.3 s	30
0.2 s	65

investigations, because of the unprecedented time resolution for a rotating gantry scanner only surpassed by EBT-scanner technology (electron beam tomography). It demonstrates the big step forward being made in noninvasive cardiac imaging. An impressive image of the heart taken at 0.37 s revolution time given in Fig. 13 underlines the possibilities today and demonstrates the strong demand for further improvement of temporal resolution. The field trial clearly confirmed, that the ball bearings no longer cause tube failures even at the high centrifugal forces. Here, the small tube with the low weight of only 3.6 kg for the entire tube and the lubrication of the bearings resulted in no observed breakdown due to bearing failure. This has to be seen in direct contrast to conventional rotating anode tube technology, where bearings inside the vacuum are difficult to lubricate, because of high operating temperatures.

The overall increased lifetime capability could of course not be demonstrated during the short trial period. However, we observed a significant lower number of high voltage breakdowns (mainly because there are no moving parts in the vacuum) and a lower focal track degradation resulting in a more constant x-ray output comparable to conventional tubes.

V. CONCLUSIONS AND FUTURE DEVELOPMENTS

From all the physical and technical aspects discussed before, some conclusions for future developments can be drawn.

(1) Although the demand for a clinical workflow not limited to cool down times at any situation is a strong driver for the convectively cooled tube technology, the clinical applications still will ask for further improvement in temporal resolution for cardiac scanning and will need faster rotating gantries in consequence. Table II shows the centrifugal forces for future CT machines, assuming a tube axis at a 650 mm radius from the center of rotation. Running now at about 20 g the next generation of scanners will perform 0.3 s per revolution being not the end of the scanner development. We demonstrated that the rotating envelope technology is the

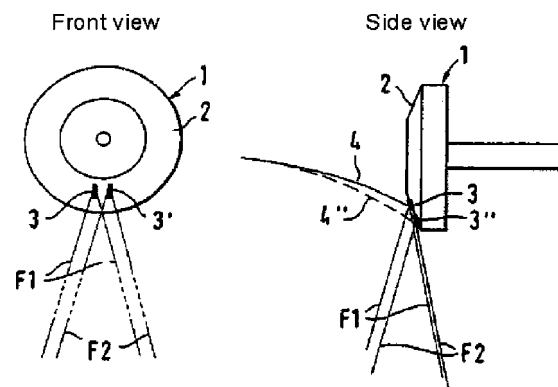


FIG. 14. Flying focal spot with the magnetic deflection system not only in ϕ , but also in the z -direction. 1: anode disk; 2: focal spot track; 3: focal spot position; 4: electron beam; F1, F2: x-rays from different focal spots.

most appropriate way to cardiac CT scanning with high time resolution. This has to be seen as an alternative to larger and heavier rotating anodes carried by bearings, which are still hard to lubricate in vacuum. Maybe the EBT (electron beam tomography) technology is comparable with respect to time resolution, but suffering from other known disadvantages.

(2) The microcontroller on board opens new possibilities to improve image quality in computed tomography. In combination with the magnetic deflection system, the microprocessor controls the beam in two directions of space at the focal spot position. Besides the already mentioned focal position stabilization, one is now able to create a flying focal spot not only within the plane of the gantry rotation (the left side of Fig. 14), but also in the radial direction¹³ (the right side of Fig. 14). This opens the opportunity to acquire twice the number of slices per revolution with a given detector, because due to the anode angle a radial movement of the focal spot corresponds to a shift of the focal spot position in z (patient axis). Moreover, the microcontroller can monitor tube performance and wear out of components in order to predict the remaining tube lifetime.¹⁷ Knowing this number, service calls can be scheduled for a tube exchange without disturbing the clinical workflow.

(3) In times of compact electronics and solid state detectors, the anode diameter of the x-ray tube mainly determines the size of a CT gantry. Here the RET technology with its smart tube housing assemblies opens a way to compact gantry design. It enables larger bores and a better patient accessibility as a future benefit for users.

^{a)}Electronic mail: peter.schardt@siemens.com

^{b)}Now at BSH Bosch und Siemens Hausgeräte GmbH, Product Area Refrigeration, Giengen, Germany.

¹H. Bittorf, in *Imaging Systems for Medical Diagnostics*, edited by E. Krestel (Siemens AG, Berlin, 1990), p. 234.

²G. Lavering and R. Treseder, Varian Associates, US Patent 5,689,542, 1996.

³C. Gerthsen, H. Kneser, and H. Vogel, in *Physik*, edited by H. Vogel (Springer-Verlag, Berlin, 1989), p. 219.

⁴T. Schmidt and R. Behling, *Medica Mundi* **44/2**, 50 (2000).

⁵Website of TOSHIBA Medical Systems, Megacool™ X-ray tube, <http://www.medical.toshiba.com/clinical/radiology/aquilionmulti16-360-360-431.htm>, 2004.

⁶W. Coolidge, General Electric Company, US Patent 1,215,116, 1917.

⁷K. Stephan, in *Taschenbuch für den Maschinenbau*, edited by W. Beitz and K.-H. Grote (Springer-Verlag, Berlin, 1997), p. D29.

⁸G. I. Taylor, *Proc. R. Soc. London, Ser. A* **151**, 494–512 (1935); *ibid.* **157**, 499–523 (1935); *ibid.* **157**, 565 (1936).

⁹H. Schlichting and F. W. Riegels, *Grenzschicht-Theorie*, Braun-Verlag, 8. Aufl., pp. 491–513 (1982).

¹⁰See, for example, J. E. Burke, L. Miller, and S. G. Perno, Picker International Inc., US Patent 5,274,690, 1993.

¹¹J. Großer, *Einführung in die Teilchenoptik* (B. G. Teubner, Stuttgart, 1983), p. 124.

¹²E. Lenz, P. Rother, and P. Schardt, Siemens AG, patent pending (to be published).

¹³E. Hell, D. Mattern, and P. Schardt, Siemens AG, US Patent 6,115,453, 2000.

¹⁴E. Hell, D. Mattern, and P. Schardt, Siemens AG, US Patent 6,292,538, 2001.

¹⁵E. Hell, D. Mattern, and P. Schardt, Siemens AG, US Patent 6,181,771, 2001.

¹⁶E. Hell, T. Ohrndorf, and P. Schardt, Siemens AG, US Patent 6,084,942, 2000.

¹⁷J. Deuringer, P. Schardt, M. Schild, and J. Freudenberger, Siemens AG, patent pending (to be published).